Wall shear stress imaging using micro-structured surfaces with flexible micro-pillars

by

Ch. Brücker[(1)] , J. Spatz[(2)] and W. Schröder[(1)]

[(1)]Aerodynamisches Institut der RWTH Aachen,
Wüllnerstr. 5-7, D-52062 Aachen, Germany
bruecker@aia.rwth-aachen.de
[(1)]Physikalisch-Chemisches Institut, Universität Heidelberg
INF 253, 69120 Heidelberg, Germany

ABSTRACT

One of the still unsolved challenging tasks in experimental fluid mechanics is the measurement of the temporal and spatial distribution of the wall shear stress. This relies on the small forces per unit area acting along the surfaces which therefore requires an excellent resolution and signal-to-noise ratio of the sensor. While single-point sensors with various conceptual principles have been successfully applied to simple canonical flows as the flow over a flat plate, there doesn't exist any quantitative picture of the spatial and temporal wall shear stress distribution as induced by coherent structures in turbulent flows. This is of fundamental interest and an important and necessary information for any implementation of reactive control of wall-bounded flows and. In the last decade micro-fabrication has offered the opportunity to scale down the devices such that there is the realistic hope to reach the high demands on spatial and temporal resolution sometimes in the future.

The new sensor concept presented herein is a micro-fabricated film-type sensor with a dense array of flexible micro-pillars which protrude from the wall into the very near-wall flow region (viscous sublayer) and bend in reaction to the applied fluid forces and the internal elastic strain. The wall shear stress distribution is determined by optical detection of the pillar bending in magnitude and direction (see also Brücker et al. 2004) and applying the relation of the wall-shear to the mean velocity gradient at the wall. The pillars with diameters of a few microns are manufactured from elastomers (e.g. poly-dimethylsiloxane PDMS) such that they are very flexible and easily deflected by the fluid forces. An example of such micro-fabricated structures with arrays of pillars is shown in Fig. 1.

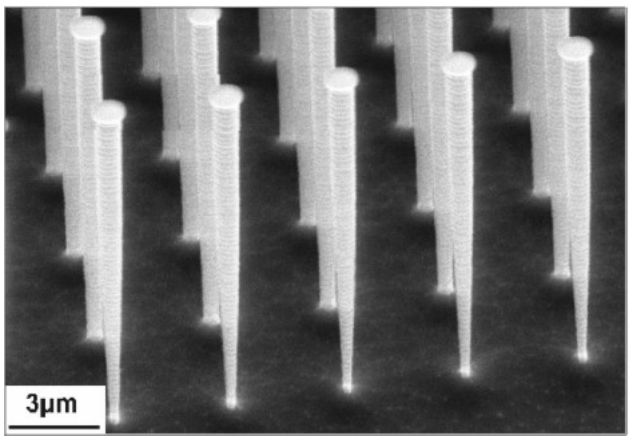

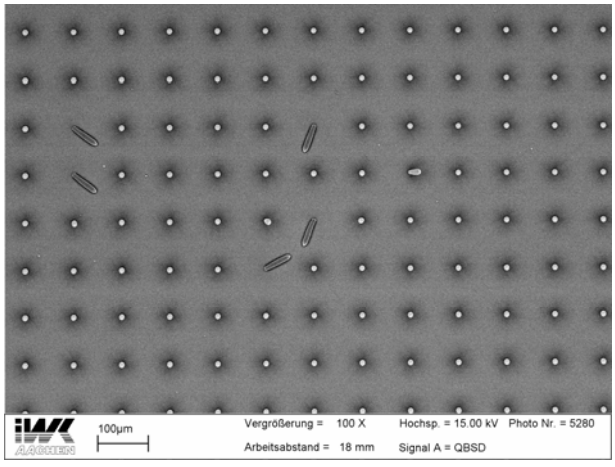

Fig. 1a): REM image of an example of micro-fabricated micro-pillars as used in biochemical cell studies (substrate: silicon, manufacturing technique: reactive ion-etching)
Fig. 1b):REM image of the sensor-film with flexible micro-pillars for wall-shear stress imaging (substrate: poly-dimethylsiloxane, manufacturing technique: negative photoresist and casting)

INTRODUCTION

Pillar arrays as shown in Fig. 1a) made of silicon were recently used in one group of the authors to study bio-functional filament systems in which the filaments are bond at the needle tips in a well defined arrangement (see Fig. 1a, Roos et al. 2003). This method offers a new area of experiments since the access is not impeded by surfaces. In addition, the micro-needles can be used as cantilever beams to measure the intra-cellular forces in the attached cells (Roy et al. 2002, Weeks et al. 2003).

For aerodynamic applications, the concept of a sensor-film with flexible micro-pillars made from PDMS as shown in Fig. 1b) opens a new area of experimental time-resolved wall shear stress measurements over larger areas within a dense array of sensors which can be detected simultaneous by optical high-speed imaging. A different approach has recently been presented by Baar et al. (2003) designing an artificial wind hair with a stiff cantilever which is fixed on a spiral spring suspension. A capacitive read-out principle is proposed and first prototypes are currently being fabricated. Similar approaches to design artificial wind hairs were published earlier by Osaki (Osaki et al. 2000) and by the group of Chen (see e.g. Chen et al. 2003). The sensory hair in Osaki's prototype was about 1500µm in length with a single hair on one chip. The angular deflection of the stiff cantilever is measured at strain gauges fabricated at the bottom of the hair. Chen et al used a flat plate with a size of 180µm×1100µm which is flapped from the base into the flow and the drag is measured with a strain gauge at the base, too. A similar sensor principle is used by von Papen et al. (2002) to measure the wall shear stress fluctuations at a single point with frequencies up to 1 kHz. The MEMS surface fence sensor consists of a 5mm long, 100-300 µm high and 7-10 µm thick silicon fence of which deflection is being transformed into an electrical signal which is proportional to the component of the wall-shear-stress perpendicular to the fence. Since all these methods use an electronic read-out principle at the bottom of the sensors which needs certain space to integrate the electronics, the size and spacing of the sensor elements is usually large compared to the micro-pillar arrays presented herein. Furthermore, these devices are more critical with respect to contamination, fouling and eventual cracking. In addition, the rigidity of the sensor restricts the use only on planar surfaces with low curvature radii. In contrast, the flexible sensor-film with the micro-pillars can be used also on curved surfaces and in rough environmental conditions since PDMS has unique chemical and physical attributes as a low glass transition temperature (T_G -125°C), a unique flexibility (the shear modulus G may vary between 100kPa and 3MPa), usability over a wide temperature range (at least from -100°C up to +100°C) and a very high notch impact strength (Lötters et al 1997). In summary, these attributes gives the new sensor concept a unique potential in experimental aerodynamics.

1. FABRICATION OF THE SENSOR

The micro-pillars were made of transparent PDMS with a Young's modulus of $E \approx 0.1\times10^6$ N/m^2. The PDMS is cast in a master form which is manufactured in a negative photolithographic process, see Fig. 2a). After being cured the sensor film is peeled off. As can be seen from Fig. 2b) it happens that some of the pillars are being overstretched at the base during peel-off which thereafter fold and adhere to the surface. These damaged pillars let recognize their form in the REM image, see Fig. 1b, demonstrating that we could achieve micro-pillars with an approximate cylindrical shape with a diameter of $D \approx 8$µm and an aspect ratio of about $L/D \approx 8$. The micro-pillars are arranged in a 2-D array with an equidistant spacing of about 95µm and the overall sensor area is 2cm × 2cm. Finally, the pillars are sputtered with gold to enhance the reflectivity on their heads. Sensor-films with these micro-pillars are referred in the following as type "A".

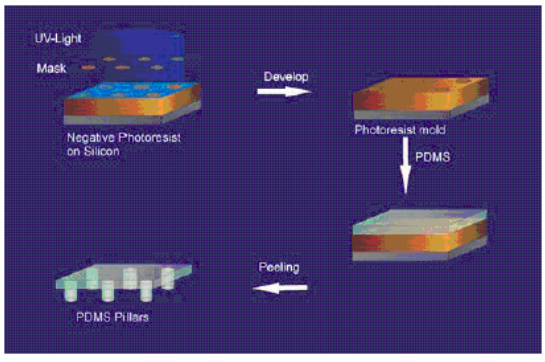

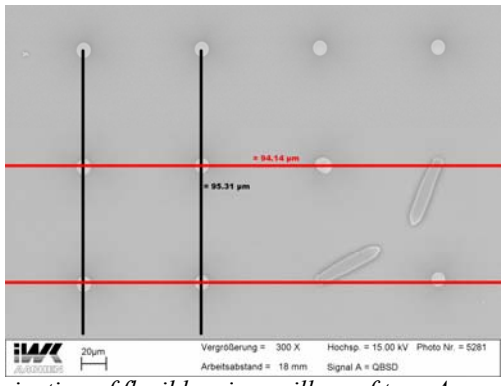

Fig. 2a): Processing steps for the -fabrication of flexible micro-pillars of type A
Fig. 2b):Dimensions and spacing of the pillars type A

Recently, we developed an alternative way to fabricate the micro-pillars using thin wax-films leaned upon the technique presented by Sitti (Sitti 2003) which is in the evaluation phase to be patented. Using this technique we could achieve a film with pillars as indicated in Fig. 3b below. The pillars have the shape of a semi-hyperboloids with a rounded tip. Most of the pillars are well formed with a surface roughness in the nano-scale. Ongoing research is concentrating on smaller holes with high aspect ratio and improved pillar-tip labelling methods. Sensors-films with these pillars are referred as type "B".

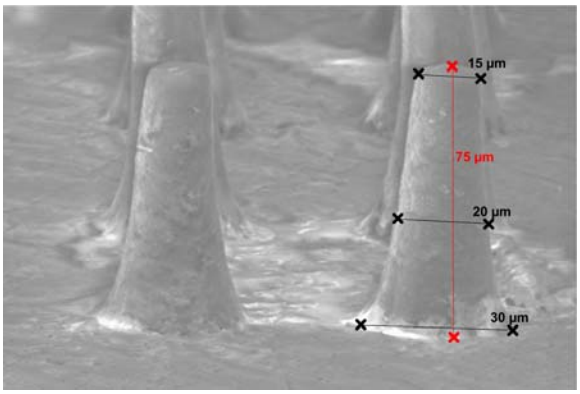

Fig. 3:Dimensions and spacing of pillars type B cast cast from wax-films
(the image of the pillars is flipped up-down to illustrate the pillar orientation on the sensor film)

2. REQUIREMENTS IN TURBULENT FLOWS

Frequency characteristics

The achievable resolution of the wall shear stress mainly depends on the diameter and aspect ratio of the pillars and is limited by the technological constraints of the micro-fabrication process and the Young's modulus E of the material. In order to estimate the necessary sensitivity and the frequency response of the micro-pillars for measurements in turbulent flows, we consider a typical flat plate boundary layer flow at Re_θ =4000. The Kolmogorov length scale is of order of 100µm and the energy spectra shows that the energy content above 10 kHz is almost negligible, therefore the sensor should resolve a frequency range between 10Hz up to a maximum of 10 kHz. The eigen frequency of a one-sided clamped rod with a length of L and a diameter of D is

$$f_i \approx D\,\lambda_i^2 \sqrt{\frac{E}{12\,\rho\,L^4}} \qquad (1)$$

with the eigen value λ_i = 1.875 yielding frequencies of the order of 10 MHz for the given geometries and properties of the pillars, much higher than the expected frequencies in turbulent flows.

Maximum pillar height and validity of linear load

With a typical length $L \approx$ 60-80µm as shown in Fig. 2,3 the micro-pillars almost stand completely submerged within the viscous sublayer which is $y \leq 5y^+$ for most of the practical turbulent flow situations to be investigated. The velocity profile near the wall in turbulent flows can be approximated as linear up to wall distances of $y \leq 5y^+$ for both U^+ and u_{rms}^+, see the Taylor expansions shown in eq.(2) and (3) (Bernard & Wallace 2002):

$$\overline{U}^+(y^+) = y^+ - \frac{(y^+)^2}{2R_\tau} + \cdots \tag{2}$$

$$\frac{u^+_{rms}}{\overline{U}^+} = 0.4 + y^+\left(\frac{0.2}{Re_\tau} + 0.07\right) + \cdots \tag{3}$$

Pillar bending in the viscous sublayer

The Reynolds number $Re = \eta\, U(L)\, D / \rho$ defined with the pillar diameter D and the maximum velocity $U(L)$ at the pillar head is in general Re ≤ 1 because of the micro-scale of the pillars. Under such conditions the pillar deflection s at the head can be estimated considering the pillar as a one-sided clamped cylinder which is bend by the viscous action of the flow described by the Oseen solution. The drag coefficient is integrated over the pillar length with the linear axial velocity profile, see also the application in microtubuli in Venier et al. 1994 which gives a first approximation of the pillar tip deflection to:

$$\left(\frac{s}{L}\right) \approx \frac{11.7\,\eta\,\dot{\gamma}}{E\,ln(L/2D)}\left(\frac{L}{D}\right)^4 \tag{4}$$

with the fluid viscosity η, the shear rate $\dot{\gamma}$ and the Young's modulus E. The equation demonstrates that the pillar deflection at the tip is directly proportional to the wall shear. Beside that, the equation proves that the relative deflection does mainly depend on the pillar aspect ratio and the flexibility.

The bending of the pillars in the near wall flow can be simultaneously determined for all pillars by high-speed imaging of the illuminated pillar heads. The pillar heads are recorded as bright spots with an approximate gaussian intensity distribution, see section 3. The centre positions of the bright spots on the image plane are detected by image processing routines with subpixel accuracy. If we assume a displacement resolution of the order of 1µm which is similar to the resolution of other optical measurement techniques relying on the detection of small gaussian spots (like Particle-Image-Velocimetry) the minimum resolvable wall friction value results to $\tau_w \approx 20$ mPa. The equivalent point force exerted on the pillar head can be detected down to 50 pN. With smaller structures than that obtained herein one can expect even smaller resolution limits.

Estimation of flow interference of the pillars

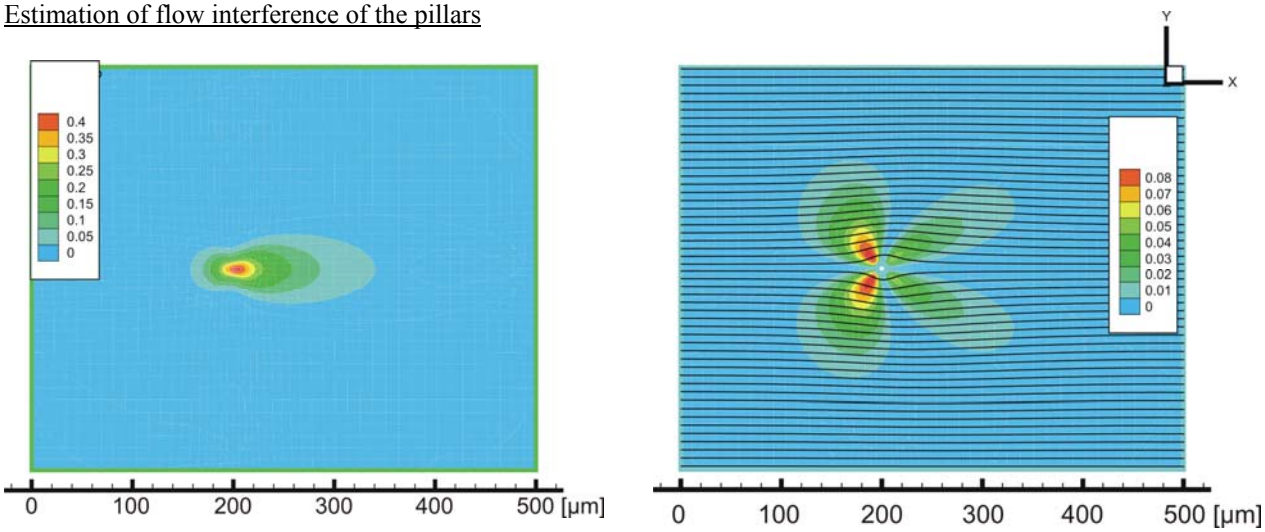

Fig. 4: Viscous flow around a single rigid pillar at Re=0.1. left: deviation of the axial velocity component from the undisturbed value at inflow $u_{mean}(L)$; right: amount of lateral velocity relative to $u_{mean}(L)$

The flow disturbance induced by the pillars itself is estimated from a numerical simulation of the Navier-Stokes Equations for a 3-D steady viscous flow around a small wall-bounded rigid pillar of a diameter of $D=10\mu$ and $L=100\mu$ in a simple planar shear flow with $\dot{\gamma}$=1000/s. The Reynolds-number defined at the pillar tip with the undisturbed axial velocity equals $Re=0.1$ for a water-glycerine mixture with a viscosity of 10cP. Exemplary results are shown in Fig. 4 in the wall-parallel plane crossing the pillar tip which indicate that the flow disturbances are died out to less than 5% of the undisturbed velocity $u_{mean}(L)$ for a radius greater than 10 pillar diameters.

Calibration procedure

Because of possible non-uniformities of the pillars we are currently underway to calibrate the sensor-film in a defined shear flow to determine the individual flexural stiffness of each individual pillar. Therefore we place the sensor flush-mounted in a cone-plate type viscometer and the bending is imaged and determined over a series of different shear velocities. The flow in the cone-plate viscometer exhibits a simple planar shear flow with constant shear as in the viscous sublayer of a turbulent wall-bounded flow. First results let recognize that non-uniformities of the pillar deflection are mainly caused by variations in the height of the pillars while the diameter is well reproduced for all pillars on the sensor-film. However, since the height of each pillar can be easily measured otherwise, the calibration procedure can be simplified in future by only measuring one single probe of a pillar and calculating the sensitivity with the individual height of each pillar.

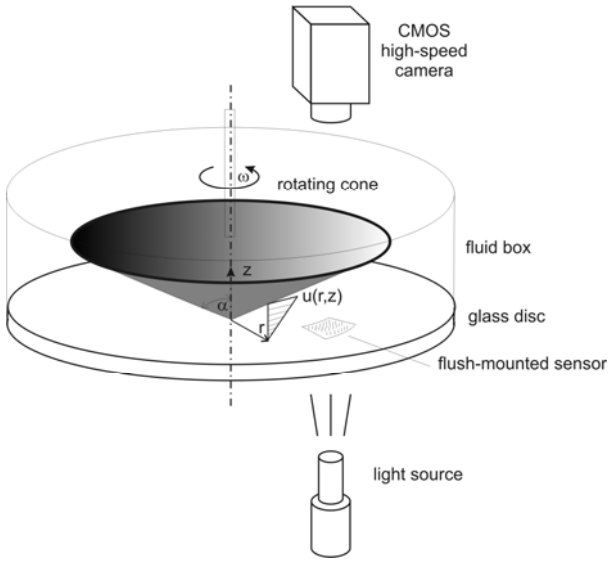

Fig. 5: Calibration procedure of the sensor-film with the micro-pillars in a defined shear flow(the cone and plate are both transparent to have all possibilities of optical access onto the sensor)

3. EXPERIMENTS

Experimental test conditions

The tests were carried out in a special designed transparent flow channel with different fluids (deionised water, a water-glycerine mixture at 50%vol with a viscosity of 10 cP and a refractive index of n=1.43, coal oil with a viscosity of 36 cP and a refractive index of n=1.43) at varying Reynolds numbers ranging from laminar to turbulent channel flow. The flow channel has a quadratic cross-section (H=50mm) and a length of 2 meters, see Fig. 5. The sensor itself is flush-mounted at the wall of an adjustable smooth rectangular constriction which is placed at a distance of 30×H downstream of the entrance. The sensor can be illuminated from top, bottom and through the sidewalls, the viewing direction is from the bottom. In some of the experiments a cylinder was placed upstream of the sensor as a defined flow disturbance.

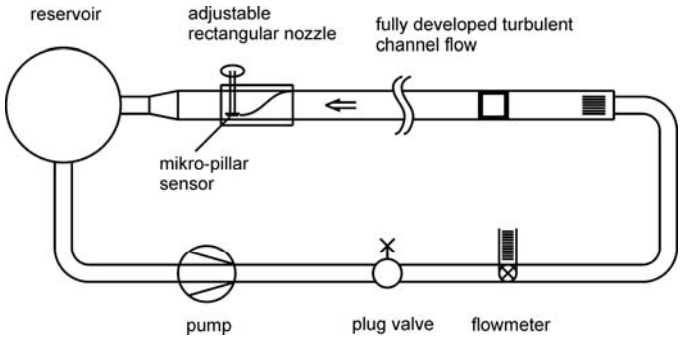

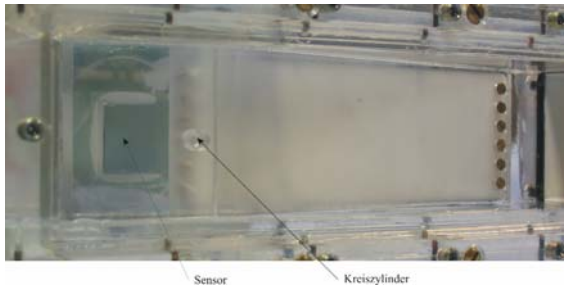

Fig 6a): Principle sketch of the test flow channel
Fig. 6b): View from bottom into the contraction zone with the sensor-film and the cylinder upstream (flow is from right to left)

Recording

The illumination and quality of the images of the pillar heads is the most crucial parameter defining the resolution limit of the pillar bending and therefore the resolution of the wall shear stress values. The first experiments let recognize an immediate wash-off of the gold at the pillar heads and therefore a strong reduction of the reflectivity during the first use in the flow channel (actually this problem could be solved for the most recent generation of sensor-films, see section Summary and Outlook). The visibility is even more a problem if the refractive index of the working fluid is close to that of the transparent pillars, e.g. when using water-glycerine or coal oil as working fluid (PDMS has a refractive index of about 1.45). In this situation, the most effective imaging of the pillar heads was achieved when illuminating with parallel light from the back of the transparent sensor film and viewing direct onto the tips of the pillars. Herein the fact is used that the transparent pillars act as optical fibres. The light is transmitted due to total internal reflection through the pillar to the rounded tip where it is coupled out and recorded as a small bright spot on the imaging sensor. The base of the pillar is seen as a larger dark circular area over a lightened background, see Fig. 7b.

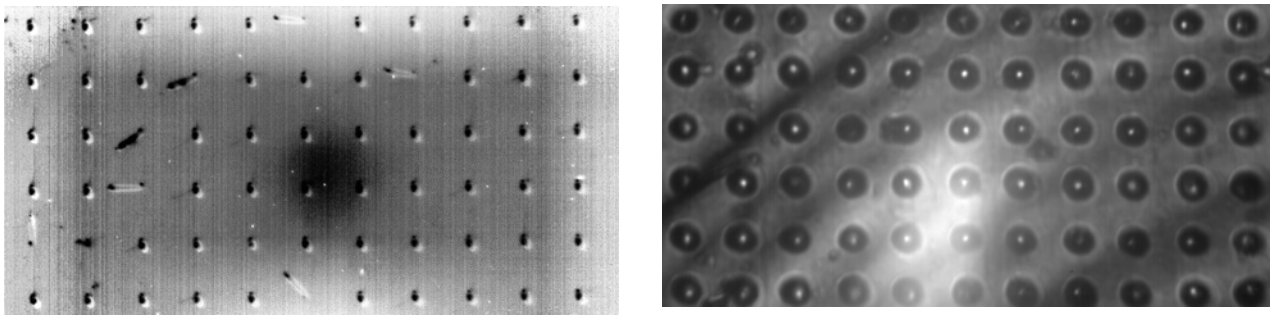

Fig. 7: Images of the different sensors in flow (left: pillars of type A with illumination from side; right: pillars of type B with backlight illumination)

For time-resolving imaging of the spatial displacements of the pillar heads we used a CMOS high speed camera (Vosskühler HCC1000, maximum frame rate 2000 frames/sec, pixel size: 6.7µm × 6.7µm) equipped with a telecentric microscopic lens with a magnification M=10 and an aperture of 0.4 (Sill Optics). The telecentric lens has two important features which are useful herein, first the telecentric imaging ensuring a constant magnification over a certain depth of focus (approximately 100µm) and second the large working distance of the lens with 38 mm which allows to focus onto the sensor at different positions of the adjustable nozzle. The diffraction limited spot size of the microscope lens is of the order of 30µm (see Meinhard et al.) and the resolution power of order of 1µm. Other than in micro-PIV, the resolution limit and therefore the accuracy of the measurements herein is solely given by the resolution power of the lens and the achievable accuracy in determining the spot position on the pillar tip with subpixel accuracy.

Image processing and evaluation

The centre positions of the pillar base and tip were determined in two successive steps with subpixel accuracy. First we determine the base positions of the pillars using the circular Hough Transformation with the a priori known image diameter of the pillars. The transformation is applied to small sub-windows centred on the regular grid of the pillars which was roughly estimated from the average pillar spacing. The original images are therefore filtered with a median filter, inverted and finally, the canny filter is applied to detect the edges. The result of the Hough transformation in each sub-window is correlated with a 2-D gaussian function and the maximum in the correlation plane is determined using a 2-D gaussian fit. This provides the coordinates of the base of the pillars with subpixel accuracy.

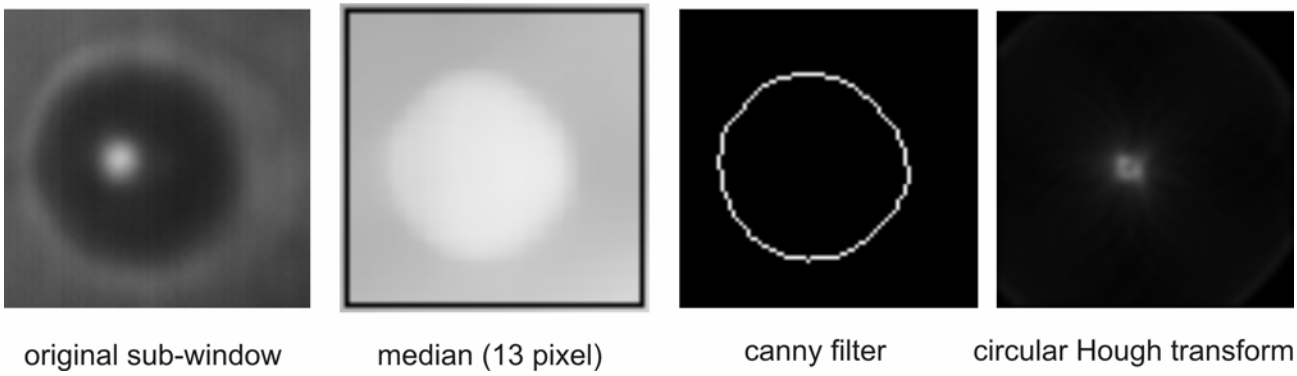

Fig. 8: Image processing steps to determine the base position and the tip of the pillars

These coordinates are used to correct for the overall sensor-film motion due to unavoidable channel vibrations. In the second step a cross-correlation method with a gaussian template mask is applied to determine the centre position of the bright spots at the pillar tips with subpixel accuracy. With subpixel interpolation methods one can achieve a minimum displacement resolution of the order of 1/5 pixel. This results in a detection limit of about 50nm of the deflection of the pillar head.

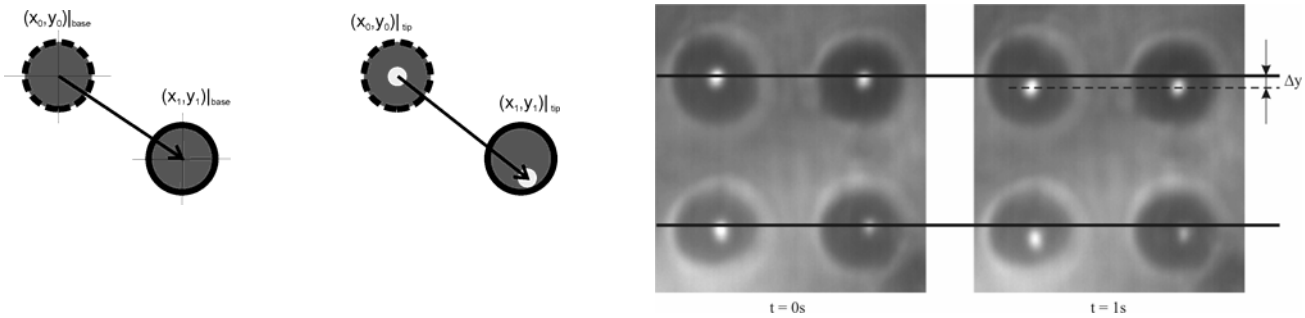

Fig. 9a): Correction for the overall sensor-film motion using the images of the pillar base at rest (x_0,y_0) and with flow (x_1,y_1) and determination of the pillar tip position.
Fig 9b) Motion-corrected images of the pillars for the channel at rest and after start of the flow in a selected area

The resolution limit of the measurements can be estimated from measurements of the pillars at zero flow and with artificially induced channel vibrations. For the given recording conditions we obtained a mean rms-value of 0.15 pixel. This includes both the inaccuracy in the determination of the pillar base position and the pillar tip position.

4 RESULTS AND DISCUSSION

The first experiments were carried out with coal oil as working medium to obtain a larger deflection of the pillars. For these conditions the flow is almost laminar. Because of the rapid wash-off of the gold at the pillar heads a strong reduction of the reflectivity happened which made the optical detection of the smaller pillars with the high-speed camera difficult, also because of the low sensitivity of the camera and the huge amount of light which is necessary. An improved labelling process is currently tested which will result in much better light efficiency. In case of the smaller

pillars, the recording frequency was therefore reduced from 500 fps down to 50 fps for the benefit of a much better visibility of the pillar heads. Fig. 9 displays the streamwise deflection s_y of the pillars after sudden start of the flow. As the flow approaches a constant value for frame no. ≧ 40 the maximum value of pillar deflection reaches values of $s \approx$ 12µm. Accidentally, a small air bubble was trapped below the sensor which helped to indicate the fluid motion. As can be seen in Fig. 10b the bubble accelerates and moves smoothly around the pillars as the boundary layer develops. At the end of the displayed sequence (frame no. 27) it reaches a velocity of 10 mm/s. This corresponds to s equal half the value of maximum deflection in the impulsive flow step. The profile displayed in Fig. 10a let recognize the first hint of fluid motion at frame no. 21 which demonstrates the high sensitivity of the sensor. In addition, the travelling of the bubble around the pillars shows that the flow around the pillars is smooth and approximately for/aft-symmetric as expected for creeping flow around a cylinder.

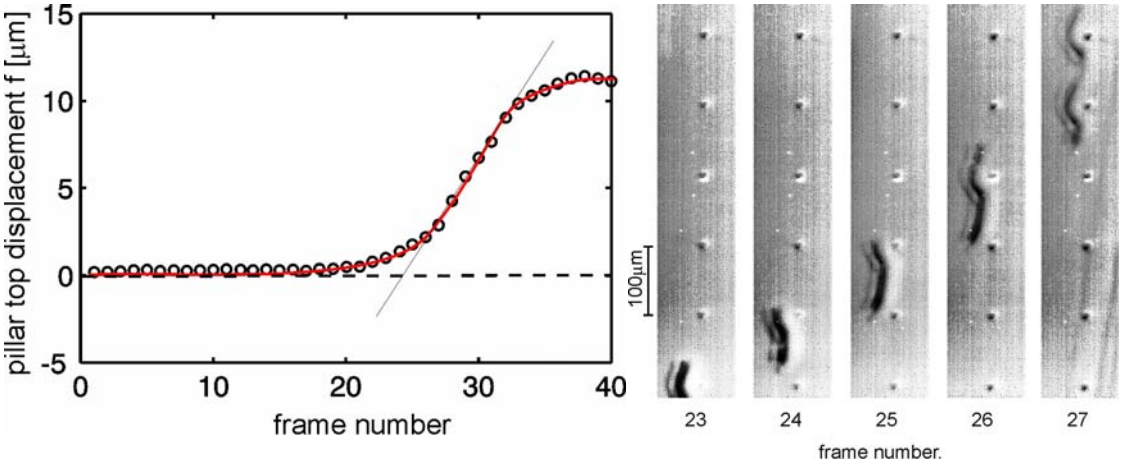

Fig. 10a): Temporal profile of average pillar displacement after sudden start of the flow (frame rate 50 fps, magnification M=10)
Fig. 10b): Motion of a small air bubble trapped underneath the sensor-film after sudden start of the flow (the flow direction in the picture is from the bottom to the top).

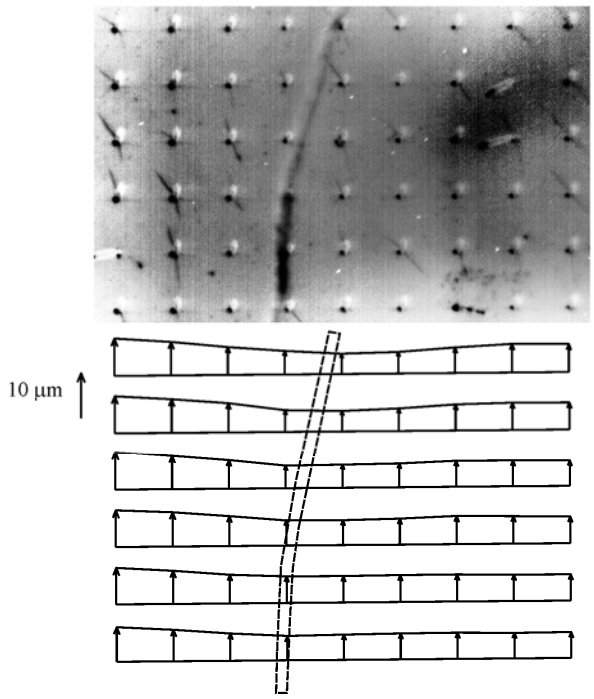

Fig. 11a): Image of the sensor-film in laminar channel flow with a small fluff tethered upstream
Fig. 11b): Pillar deflection field showing the stokes drag of the fluff influencing the near wall flow

Fig. 11 displays a special configuration in which a long fluff with a diameter of approximately 25µm was tethered upstream of the sensor near the wall. The instantaneous deflection field of the sensor-film is given by means of vectors on the regular pillar grid of which length is proportional to the measured tip deflection. As can bee seen from the original image and the measured vector field, the stretched fluff affects the flow near the wall due to the stokes drag it induces itself. Therefore, the pillars immediate below or in the near vicinity of the fluff indicate a smaller deflection. This influence is seen over a radius of about 200µm in which the wall shear profiles are disturbed.

Additional measurements were carried out with the larger pillars in the same flow configuration. Fig. 12 displays the streamwise deflection s_y of the pillars after sudden start of the flow, compare Fig. 10a. Herein, the high-speed camera recorded with 500 fps and only each third measurement point is shown. The circles represent the unfiltered raw data of each image averaged to a single value of the streamwise deflection (Fig. 12a) and the lateral deflection (Fig. 12b).

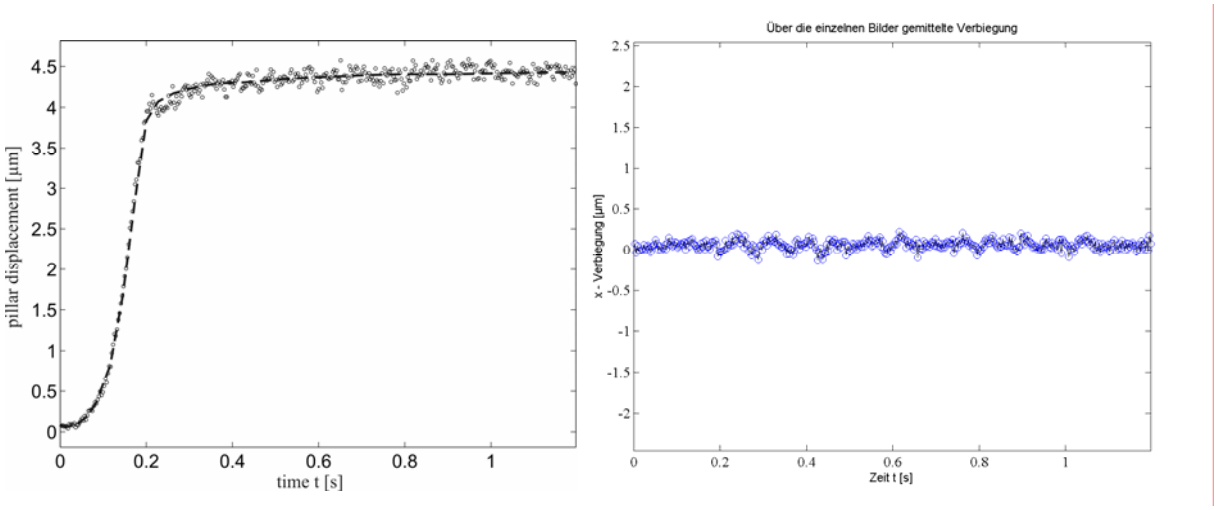

Fig. 12): Temporal profile of average pillar displacement after sudden start of the flow (frame rate 500 fps, magnification M=10); left: streamwise component; right: lateral component

Fig 12 demonstrates the high temporal resolution which can be obtained. The small fluctuations in Fig 12 are still partly correlated with the overall motion of the sensor-film. The final pillar deflection values of about 4µm are a factor of 3 smaller than those obtained for the small pillars. This relation is also predicted by equation (4) which again demonstrates the importance of the small diameter and high aspect ratio to obtain the highest resolution.

5 CONCLUSION AND OUTLOOK

The preliminary results presented herein show the feasibility of the presented sensor concept to measure the wall shear stress in time and in 2-D along the sensor surface with high accuracy and high resolution. With the described manufacturing techniques we were able to fabricate micro-pillars with a size of approximately 8µm and a height of 60 µm. An alternative way has been developed which has the potential for fabricating large flexible sensor-films. Recent progress gives hope to achieve smaller pillars with a higher aspect ratio. In addition, the usability of PDMS over a wide temperature range and a very high notch impact strength gives the new sensor a unique potential in experimental aerodynamics. Furthermore, the transparency of the PDMS and therefore of the micro-pillars has been used herein to illuminate and visualize the pillar tips. In fact, the micro-pillars act as micro-optical fibres in which the total internal reflection ensures that the light is transmitted to the tip. This fact may also be used as part of an optical read-out sensor principle (patent pending). Ongoing measuring campaigns are planned for a transitional boundary layer flow on a flat plate first in a large oil channel at the LSTM in Erlangen, Germany, and second in a large water channel at the AIA.

ACKNOWLEDGEMENT

The authors gratefully acknowledge the support of this project by the Deutsche Forschungsgemeinschaft DFG in the priority program “Nano & Microfluidics”. In addition, the authors thank Dr. Schmitz, Dipl.-Ing. Jacobs and Dipl.-Chem. Ulmer for the manufacturing of the sensor-films. Finally, many thanks to Mr. Triep for carrying out the numerical simulations and Mr. Mohr from IWK for the REM images.

REFERENCES

Bernard PS & Wallace JM: Turbulent Flow: Analysis, Measurement, and Prediction. John Wiley & Sons, Inc. 2002.

Brücker C, Spatz J, Schröder W: Wall shear imaging in turbulent flows using micro-structured surfaces with flexible micropillars. Proc. 10th EUROMECH European Turbulence Conf., 29 June - 2 July 2004, The Norwegian University of Science and Technology, Trondheim, Norway, 2004.

Chen J, Fan Z, Zou J, Engel J, Liu C: Two dimensional micromachined flow sensor array for fluid mechanical studies. Journal Aerospace Engineering 16(2), 85-97, 2003.

Lötters JC, Olthuis W, Veltink PH, Bergveld P: The mechanical properties of the rubber elastic polymer polydimethylsiloxane (PDMS) for sensor applications. J. Micromech. Microeng. 7, 145-147, 1997.

Meinhart, CD.; Wereley, ST.: The theory of diffraction-limited resolution in microparticle image velocimetry. Meas. Sci. Technol. 14, 1047–1053, 2003.

Osaki Y, Ohyama T, Yasuda T, Shimoyama I: An air flow sensor modelled on wind receptor hairs of insects. Proc. MEMS 2000, 531-6, 2000.

Roos W, Roth A, Konle J, Presting H, Sackmann E, Spatz J: Freely suspended Actin cortex models on arrays of micro-fabricated pillars. Chem. Phys. Chem.4, pp. 872-876, 2003.

Roy P, Rajfur Z, Pomorski P, Jacobson K: Microscope-based techniques to study cell adhesion and migration. Nature cell biology 4(4), pp. E91-E96, 2002.

Sitti M: High Aspect Ratio Polymer Micro/Nano-Structure Manufacturing using Nanoembossing, Nanomolding and Directed Self-Assembly. IEEE/ASME Advanced Mechatronic Conf. , Kobe, Japan, July 2003.

Van Baar JJ, Dijkstro M, Wiegerink RJ, Lammerink TSJ, Kijnen: Fabrication of array of artificial hairs for complex flow pattern recognition. Presented at the IEEE Sensor Conference, Toronto, October 22-24, 2003.

Venier P, Maggs AC, Carlier MF, Pantaloni D: Analysis of microtubule rigidity using hydrodynamic flow and thermal fluctuations. J. Biol. Chem. 269, 13353-13360, 1994.

Von Papen T, Buder U, Ngo HD, Obermeier E: High resolution wall shear stress measurement using a MEMS surface fence sensor. Proc. Eurosensors XVI, September 15-18, 2002, Prague, Czech Republic, pp. 744-747, 2002.

Weeks B, Camarero J, Noy A, Miller A, Stanker L, De Joreo J: A micro cantilever-based pathogen detector. Proc. Nanotechnology Conf. Nanotech 2003, Febr. 23-27, San Francisco, 2003.